

A Style-Based Profiling Framework for Quantifying the Synthetic-to-Real Gap in Autonomous Driving Datasets

Dingyi Yao, Xinyao Han, Ruibo Ming, Zhihang Song, Lihui Peng, Jianming Hu, Danya Yao, Yi Zhang

Abstract—Ensuring the reliability of autonomous driving perception systems requires extensive environment-based testing, yet real-world execution is often impractical. Synthetic datasets have therefore emerged as a promising alternative, offering advantages such as cost-effectiveness, bias free labeling, and controllable scenarios. However, the domain gap between synthetic and real-world datasets remains a major obstacle to model generalization. To address this challenge from a data-centric perspective, this paper introduces a profile extraction and discovery framework for characterizing the style profiles underlying both synthetic and real image datasets. We propose Style Embedding Distribution Discrepancy (SEDD) as a novel evaluation metric. Our framework combines Gram matrix-based style extraction with metric learning optimized for intra-class compactness and inter-class separation to extract style embeddings. Furthermore, we establish a benchmark using publicly available datasets. Experiments are conducted on a variety of datasets and sim-to-real methods, and the results show that our method is capable of quantifying the synthetic-to-real gap. This work provides a standardized profiling-based quality control paradigm that enables systematic diagnosis and targeted enhancement of synthetic datasets, advancing future development of data-driven autonomous driving systems.

Index Terms—autonomous driving, synthetic dataset, profile extraction and discovery, synthetic-to-real gap.

I. INTRODUCTION

Ensuring the safety and reliability of autonomous driving perception systems requires extensive testing and validation. Recent research emphasizes environment-based testing, which evaluates system performance under diverse and dynamic conditions while revealing safety-critical risks [1]. However, conducting such testing in the real world is costly, time-consuming, and unsafe [2], [3].

To overcome these limitations, synthetic datasets generated by autonomous driving simulation platforms have emerged as a promising supplementary data source [4]. These synthetic datasets construct virtual environments using advanced graphics engines. For instance, the GTA-V [5] is derived from a commercial video game environment, whereas SYNTHIA [6], Virtual KITTI [7], Virtual KITTI 2 [8] are developed using the Unity engine. Similarly, datasets such as SHIFT [9] are built upon the CARLA platform.

Compared to real-world datasets, synthetic datasets offer several notable advantages. First, they can be generated efficiently without the need for extensive time and labor-consuming data collection efforts. Second, annotations are programmatically generated with pixel-perfect precision, eliminating subjective bias that may arise in manual labeling

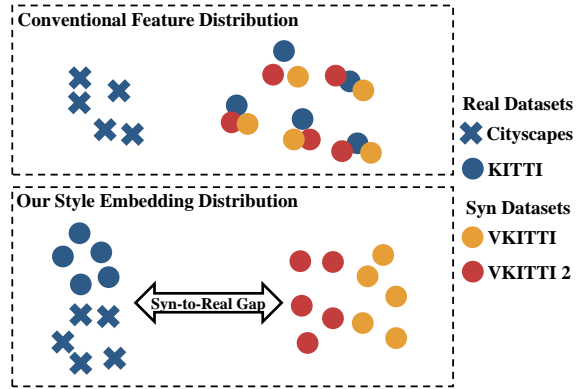


Fig. 1. Schematic of our Style Embedding Distribution Discrepancy (SEDD). Conventional feature distributions are influenced by image content, separating different real datasets while clustering real datasets with their cloned synthetic counterparts. Our approach disentangles content and style, distinguishes between real and synthetic datasets, and measures the synthetic-to-real gap.

processes. Additionally, synthetic environments enable full controllability over environmental variables, facilitating the generation of diverse scenarios. Finally, synthetic data can be targeted to generate rare scenarios critical to security verification that are difficult to capture in real world. Reflecting these advantages, prior studies have demonstrated their effectiveness in object detection and tracking [10], as well as lane detection and classification [11].

Despite the notable advantages of synthetic datasets, their application also presents new challenges, particularly in whether they support transfer to real-world scenarios. At the heart of this issue lies the synthetic-to-real gap, whose quantification is therefore crucial.

Existing methods for quantifying the synthetic-to-real gap in autonomous driving image datasets still have notable limitations. For example, common evaluation metrics include PSNR [12], SSIM [13], LPIPS [14], and FID [15]. These metrics assess quality according to the differences between generated images and their corresponding real reference images. However, synthetic datasets generated from simulation platforms typically provide only the final synthetic images without accompanying referenced real images, rendering these methods less applicable. Moreover, some studies [16]–[18] indirectly evaluate dataset quality by comparing the performance differences on downstream tasks between real and synthetic datasets. Since the label spaces of different datasets may only

partially overlap or even be entirely disjoint, these methods often have a limited scope of applicability.

To address these issues, we introduce a novel style-based profiling framework with a metric, Style Embedding Distribution Discrepancy (SEDD). The main contributions of this work are as follows:

- We innovatively model the discrepancies between synthetic and real data as differences in extracted style profiles and propose a data fidelity metric Style Embedding Distribution Discrepancy (SEDD).
- We utilize the publicly available real datasets and synthetic datasets to establish a benchmark for evaluating the synthetic-to-real gap.
- A large number of experiments have been conducted on real datasets, synthetic datasets to demonstrate the effectiveness of our proposed profiling framework.
- We apply the proposed profiling framework to sim-to-real approaches in autonomous driving, providing quantitative metrics and visualization tools for their evaluation.

II. RELATED WORK

A. NR-IQA for Single Images

Since many synthetic datasets lack real-world counterparts [5], [9], it is necessary to employ No-Reference Image Quality Assessment (NR-IQA) methods. Classical approaches such as BRISQUE [19] rely on natural scene statistics with SVM regression. With the advent of deep learning, data-driven NR-IQA methods have emerged, including NIMA [20], which employs end-to-end CNN training, and Unique [21], which leverages samples from multiple databases to achieve robust generalization.

Although these methods have achieved commendable performance in generic contexts, they may incorrectly judge real-world datasets as having inferior quality. This error arises because conventional quality assessment techniques focus solely on the visual quality of an image (“how good the quality is”), neglecting its fidelity or similarity to real-world scenes (“how realistic the image is”).

B. Synthetic Datasets Generation and Enhancement for Autonomous Driving

In the field of autonomous driving, synthetic datasets provide a new way to acquire data. One notable example is Virtual KITTI [7]. This dataset was developed by selecting five real-world video sequences from the KITTI [22] dataset as seed data, which were then cloned and modified for weather conditions in the Unity engine. Building on this foundation, Virtual KITTI 2 [8] was introduced as an enhanced version of Virtual KITTI. By taking advantage of new features available in the updated Unity engine, such as the high-definition rendering pipeline, Virtual KITTI 2 delivers improved visual effects with more realistic image details.

After the rise of synthetic datasets, a number of data enhancement efforts have been proposed, working on the algorithms that improve the fidelity, such as color transfer [23] based on statistical analysis, and CUT [24], EPE [25] based on

image-to-image translation. In addition, CARLA2Real [26], utilized photorealism enhancement technique to narrow the gap between CARLA platform and reality. The target datasets for methods CARLA2KITTI and CARLA2CITY are KITTI [22] and Cityscapes [27].

Both generated and enhanced synthetic datasets need an objective metric to assess the synthetic-to-real gap.

C. Synthetic-to-Real Gap Quantification for Autonomous Driving

Gadipudi et al. [28] proposed a method that leverages feature embedding techniques to compute the Euclidean distance between real and synthetic datasets. However, its evaluation outcomes are susceptible to variations in image content and fail to disentangle content from style. This issue is particularly pronounced in scenarios where the Virtual KITTI dataset has a one-to-one correspondence with the KITTI dataset; in such cases, the computed feature distance may underestimate the stylistic differences between the two. In addition, using unsupervised methods for dimensionality reduction before calculating distances will lead to significant information loss.

Li et al. [29] evaluated datasets using a total of 11 metrics across three dimensions: formal quality, content quality, and utility quality. However, the fact that its indicators have full scores for all datasets on multiple indicators implies redundancy in these indicators, weakening the discriminative power of the methodology. Moreover, their handcrafted features may hinder the capture of high-level semantic differences.

Duminil et al. [30] assessed the gap by extracting texture features using the gray-level co-occurrence matrix [31], local binary patterns [32], and discrete wavelet transform [33]. In their subsequent work [34], the authors introduced the Dempster-Shafer theory to enhance the evaluation model through multi-criteria fusion. Although these methods effectively reflect differences at the level of image details, their focus on texture makes them highly sensitive to environmental factors (such as weather, lighting, and scene variations). For instance, their evaluation scope is only restricted to urban scenes under clear weather conditions.

III. METHODOLOGY

The overall profiling framework is illustrated in Fig. 2. The framework takes as input real images, synthetic images under various weather conditions. During the training phase, input data is processed through a feature extractor to obtain feature maps, followed by a style extractor that generates feature embeddings. These embeddings are then processed using metric learning, incorporating Center Loss and NTXent Loss. The combined loss is propagated backward to update the parameters of the feature extractor and style extractor. In the evaluation phase, the learned feature embeddings undergo post-processing to compute fidelity metrics, providing an objective quantification of the synthetic-to-real gap.

A. Feature Extraction

We choose ResNet [35] as the backbone. To investigate the differences in feature representations across various layers of

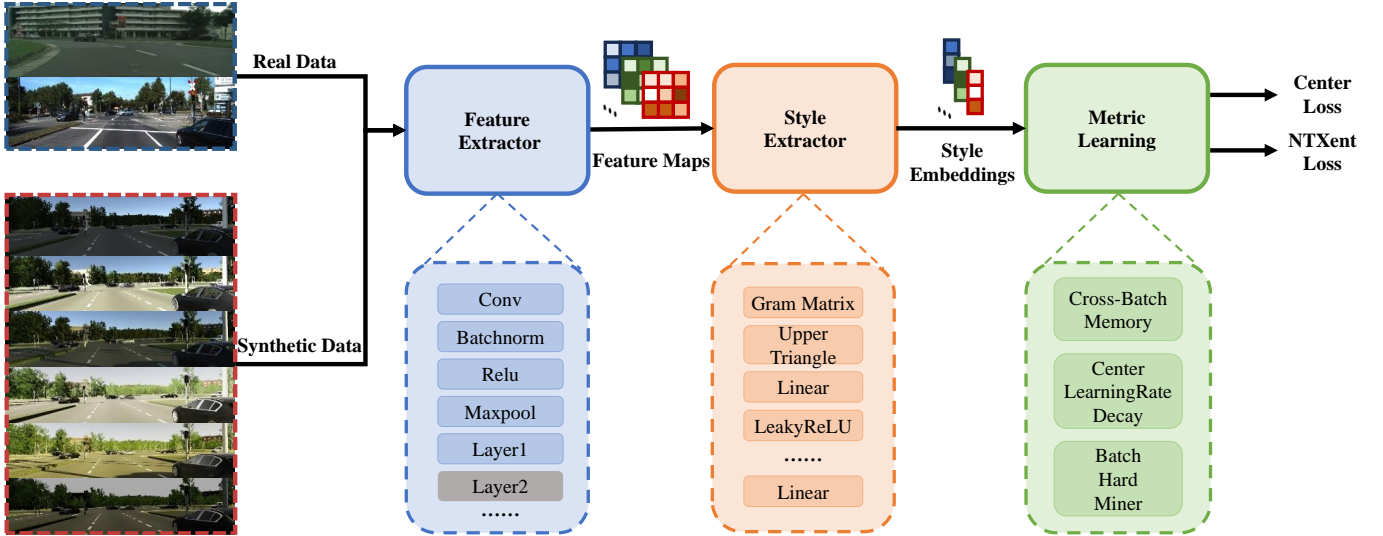


Fig. 2. The overall profiling framework. The model takes as input real images, synthetic images under various weather conditions. The input images are sequentially processed through three key modules: feature extractor, style extractor, and metric learning module. During training, the model parameters are optimized using a combination of Center Loss and NTXent Loss. In the evaluation phase, the learned feature embeddings are post-processed to compute the final SEDD metric.

the feature extractor, we choose three datasets KITTI, Virtual KITTI and Virtual KITTI 2, load pre-trained weights from ImageNet [36] and visualize the feature maps of different backbone layers. The visualization results are shown in Fig. 3. The feature maps are flattened, and then visualized using t-SNE [37]. From the figure, it can be observed that in the shallower layers of the network, points of the same color tend to cluster together. As the depth of network increases, the points representing the same scene illustrated by circles, triangles, and crosses are observed to converge. This suggests that shallower layers primarily capture stylistic features related to dataset realism, whereas deeper layers focus more on high-level semantic information, such as scene and object content within the images. Therefore, we use the shallow layer as the feature extractor. It captures style-related features while avoiding excessive extraction of content features.

Given an input image $I \in \mathbb{R}^{K \times H_0 \times W_0}$, the feature extractor \mathcal{E} produces the corresponding feature map

$$F = \mathcal{E}(I) \quad (1)$$

where the resulting feature map $F \in \mathbb{R}^{C \times H \times W}$, with C denoting the number of feature map channels.

B. Style Extraction

Inspired by domain adaptation researches [38], [39], we introduce Gram matrix [40] for style representation. Gram matrix is computed as follows: first, each feature map is flattened into a vector of shape $C \times (H \times W)$. Then, the inner product between different channels is calculated to obtain the Gram matrix, defined by

$$G_{ij} = \sum_{h=1}^H \sum_{w=1}^W F_i(h, w) \cdot F_j(h, w) \quad (2)$$

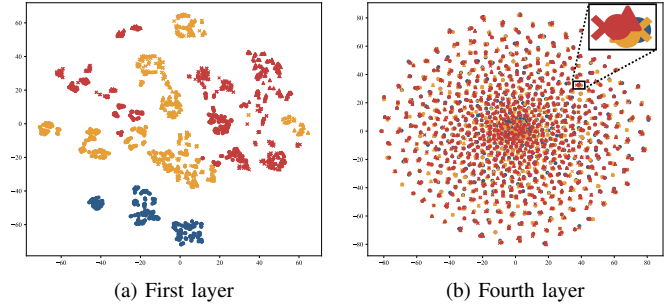


Fig. 3. Visualization of feature map from different layers of ResNet. Blue points, orange points, and red points respectively represent samples from the KITTI dataset, Virtual KITTI dataset, and Virtual KITTI 2 dataset. Different shapes (circles, triangles, and crosses) denote samples under different weather conditions in the synthetic datasets.

where G_{ij} is the Gram matrix element representing the correlation between channels i and j .

The Gram matrix captures the similarity of response patterns between different feature maps. Instead of spatial position-dependent features, the Gram matrix focuses solely on global response patterns across the entire image, making it particularly effective for capturing spatially invariant style features.

However, the number of elements in the Gram matrix is C^2 , which is prohibitively large. It can have a detrimental effect on the subsequent metric learning and loss computation. To address this, we adopt a dimensionality reduction strategy.

First, since the Gram matrix G is symmetric, its upper triangular elements can fully represent the matrix. By flattening these upper triangular elements into a one-dimensional vector, we define the Gram vector as

$$v = \text{vec}(\text{triu}(G)) \quad (3)$$

Then, the Gram vector is fed into a fully connected neural network, denoted as \mathcal{S} , where each layer consists of a linear transformation

$$z = \mathcal{S}(v) \quad (4)$$

This vector serves as the style embedding with dimension reduced from C^2 (e.g., 4096) to 64.

C. Metric Learning

The core idea of metric learning is to learn an appropriate space where samples of the same class are placed closer together, while samples of different classes are pushed farther apart.

Samples are typically divided into three categories: anchor (A), a reference sample; positive (P), from the same class as the anchor; and negative (N), from a different class. In our setting, all real datasets share a single label, while each synthetic dataset is treated as a separate label. For example, if an image from KITTI serves as the anchor, other real images act as positives, whereas synthetic images (e.g., from Virtual KITTI or Virtual KITTI 2) are considered negatives.

In order to efficiently store feature embeddings from historical batches, we propose the cross batch memory module. Notably, it only retains low-dimensional embeddings rather than raw images or Gram matrices. This design choice significantly reduces memory consumption while simultaneously enlarging the pool of samples available for metric learning.

To enforce intra-class compactness, we adopt Center Loss [41], which minimizes the distance between a sample's feature vector and its corresponding class center. It is defined as

$$\mathcal{L}_C = \frac{1}{m} \sum_{i=1}^m \|z_i - c_{y_i}\|_2 \quad (5)$$

where m is the number of samples, c_{y_i} denotes the center of the class y_i , which is a learnable parameter.

To avoid oscillations due to overly aggressive updates, we propose the center learning rate decay strategy. If the initial center learning rate is η_c^0 , then at iteration t , the learning rate is given by

$$\eta_c^{(t)} = \eta_c^0 \cdot \gamma^t \quad (6)$$

where γ is the decay factor.

Selecting informative sample pairs is crucial for effective metric learning. The batch hard miner [42] selects challenging pairs from the current memory. For a given anchor sample A_i , the hard positive sample is defined as the same-class sample with the lowest similarity to A_i

$$\arg \min_{j: y_j = y_i} \text{sim}(A_i, P_j) \quad (7)$$

where sim denotes the cosine distance. Mining such difficult pairs guides the model to focus on hard negatives, which accelerates convergence and enhances overall performance.

To explicitly maximize inter-class separability, we incorporate the NTXent Loss [43]. Given an anchor sample A_i with its positive counterpart P_j , and S_k sampled from all current samples, the loss is computed as

$$l_{ij} = -\log \frac{\exp(\text{sim}(A_i, P_j)/\tau)}{\sum_{k=1}^{2m} \mathbb{I}_{[k \neq i]} \exp(\text{sim}(A_i, S_k)/\tau)} \quad (8)$$

$$\mathcal{L}_{\text{NTXent}} = \sum_{i,j} l_{ij} \quad (9)$$

where τ is the temperature coefficient.

D. Loss Function

To jointly optimize both intra-class compactness and inter-class separability, the overall loss function is formulated as

$$\mathcal{L}_{\text{total}} = \mathcal{L}_{\text{NTXent}} + \lambda \mathcal{L}_C \quad (10)$$

where λ is a balancing factor.

E. Post-Processing

The mean vector of style embeddings is computed as

$$c = \frac{1}{m} \sum_{i=1}^m z_i \quad (11)$$

For a new synthetic dataset, let its style center be c_{new} , and let the style center of the real dataset c_{real} . The Euclidean distance between these two centers is defined as SEDD_1

$$\text{SEDD}_1 = \|c_{\text{new}} - c_{\text{real}}\|_2 \quad (12)$$

In addition, Maximum Mean Discrepancy (MMD) [44] is a kernel-based measure for quantifying the divergence between distributions of real dataset and synthetic dataset. Using a Gaussian kernel $k(x, y) = \exp\left(-\frac{|x-y|^2}{2\sigma^2}\right)$, the squared MMD statistic between finite samples is estimated and defined as SEDD_2 , calculated by

$$\begin{aligned} \text{SEDD}_2 = & \frac{1}{m(m-1)} \sum_{i \neq j}^m k(x_i, x_j) + \frac{1}{n(n-1)} \sum_{i \neq j}^n k(y_i, y_j) \\ & - \frac{2}{mn} \sum_{i=1}^m \sum_{j=1}^n k(x_i, y_j) \end{aligned} \quad (13)$$

Euclidean distance quantifies the overall deviation of the dataset's style, while MMD captures the distributional differences at a finer granularity.

IV. EXPERIMENTS

A. Experimental Setup

1) *Datasets*: Real-world datasets KITTI [22], Cityscapes [27] and synthetic datasets Virtual KITTI [7], Virtual KITTI 2 [8] are used to train our reference benchmark. For synthetic datasets, weather conditions, ‘clone’, ‘morning’ and ‘overcast’, are selected. The data is partitioned into training, validation, and test sets with a ratio of 6:2:2. Additionally, we evaluate the sim-to-real methods. The photorealism enhance series include Colortransfer [23], CUT [24], EPE [25]. CARLA2Real [26] series consist of CARLA2KITTI and CARLA2CITY.

2) *Implementation Details*: All experiments are conducted on a single NVIDIA GeForce RTX 3090 GPU. ResNet-18 [35] is selected for feature extractor backbone. The feature extractor is initialized with pre-trained weights from ImageNet [36]. The cross batch memory size is set to 100 and kernel bandwidth σ is set to 10. The model is trained for a maximum of 4 epochs, with a learning rate of 5e-5 for the feature extractor and style extractor. The hyperparameter λ is set to 0.5 and τ is set to 0.015. We use the SGD optimizer with momentum of 0.9 and weight decay of 1e-4. The initial learning rate of Center Loss is set to 10, and the decay factor γ is set to 0.9.

3) *Visualization*: We employ t-SNE [37] for visualization. For visual effect, 1000 images were randomly selected from each test dataset. It is worth noting that due to the visualization algorithm itself, even for the same data distribution, its shape may change after t-SNE with other different distributions.

B. Results and Discussions

1) *Quantification Results on Validation Set*: The results of our trained profiling framework on the validation set are shown in Table I. This result provides a reference value for subsequent quantification. Notably, during the training process, no label prior information indicating that Virtual KITTI 2 is superior was provided. Nevertheless, our profiling framework autonomously determines that the style of Virtual KITTI 2 is closer to that of the real dataset, resulting in a smaller synthetic-to-real gap. Fig. 4a presents the visualization results. In the figure, the sample points are clustered by color rather

than by shape, which indicates that our method achieves the disentanglement of content and style.

TABLE I
QUANTIFICATION RESULTS ON VALIDATION SET

Datasets	$SEDD_1$	$SEDD_2$
Virtual KITTI	0.308	0.488
Virtual KITTI 2	0.276	0.408

2) *Compared with NR-IQA*: The results are summarized in Table II, where the best performance is highlighted in bold and the second-best is underlined. The results demonstrate that NR-IQA methods do not sort correctly, while only our method correctly identifies KITTI as the most realistic and Virtual KITTI as the least realistic.

TABLE II
COMPARISON WITH NR-IQA METHODS ON TEST SET

Datasets	Brisque ↓ [19]	NIMA ↑ [20]	Unique ↑ [21]	$SEDD_1$ ↓	$SEDD_2$ ↓
KITTI	21.6	3.73	0.11	0.102	0.081
VKITTI	42.7	4.56	0.13	0.305	0.480
VKITTI2	<u>19.1</u>	<u>4.56</u>	<u>1.40</u>	0.274	0.402

3) *Quantification Results on Test Set*: The results of our model on test set are shown in Table III. ‘-’ indicates that the experiment was not performed. The $SEDD_1$ and $SEDD_2$ of the real dataset are all smaller than those of the synthetic dataset. The visualization results on the real datasets are shown in Fig. 4b and results on the synthetic datasets are shown

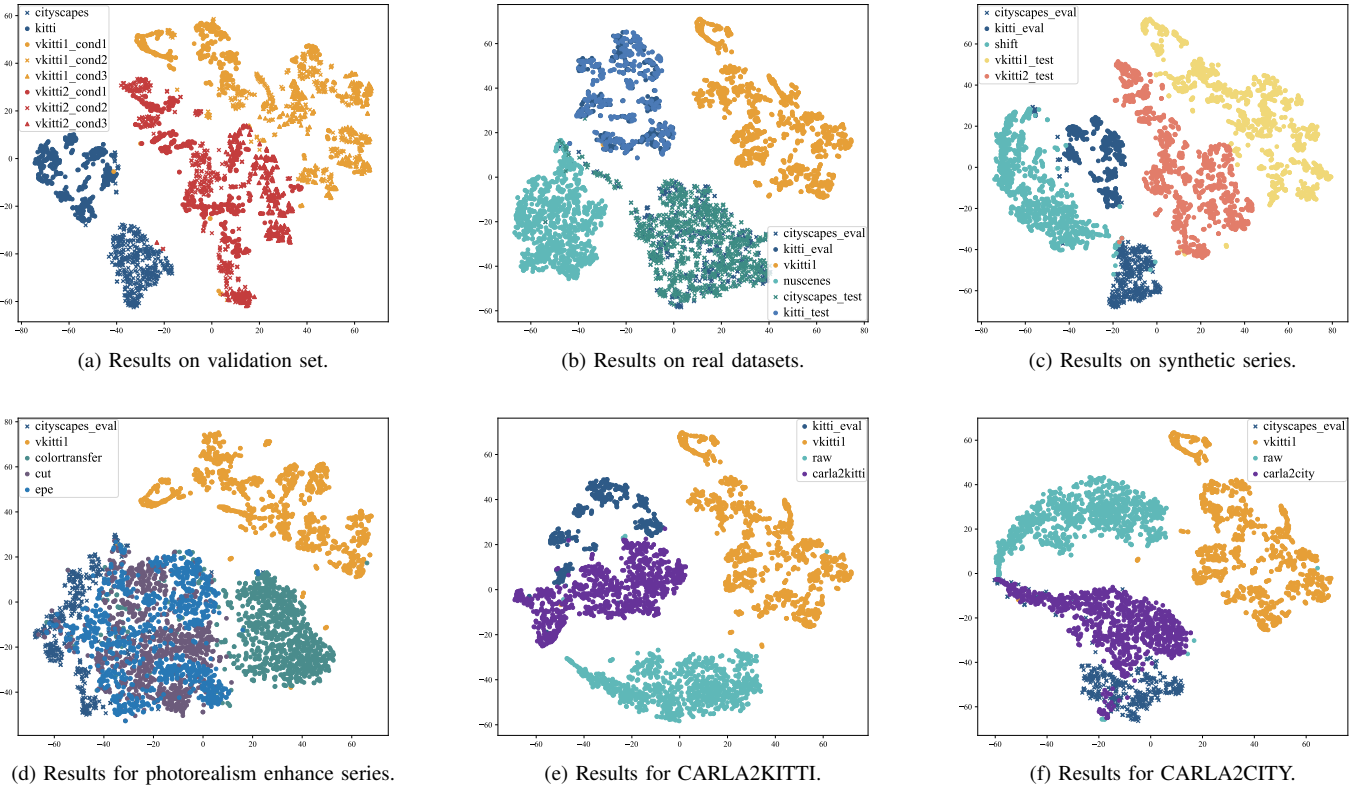


Fig. 4. Visualization of results on validation set and for sim-to-real methods. The result visually demonstrates that our profiling framework can distinguish Virtual KITTI dataset from Virtual KITTI 2 dataset. And the samples after sim-to-real are closer to the real ones.

TABLE III
EXPERIMENTS ON REAL AND SYNTHETIC TEST SET

Datasets	FE↓ [28]	Li et al. ↑ ⁵ [29]	Duminil et al. ↑ ¹⁰⁰ [30], [34]				Ours↓	
			GLCM	Wavelets	LBP	sH	SEDD ₁	SEDD ₂
KITTI [22]	-	4.845	99.81	96.85	94.87	62.42	0.103	0.085
Cityscapes [27]	4.47	-	96.67	98.05	87.46	72.76	0.122	0.111
nuScenes [45]	-	-	90.94	98.54	60.46	73.60	0.143	0.197
Virtual KITTI [7]	22.31	-	-	-	-	-	0.316	0.494
Virtual KITTI 2 [8]	-	-	0.05	51.21	02.24	34.10	0.275	0.406
SHIFT [9]	-	4.792	-	-	-	-	0.210	0.275

in Fig. 4c. Unlike other methods that have not been tested on both Virtual KITTI and Virtual KITTI 2, two datasets with extremely similar scenarios, our approach is capable of making accurate distinctions and aligns well with subjective visual assessments. Additionally, other methods rely solely on datasets captured under a single weather condition. In contrast, our method can make an effective distinction and is consistent with subjective visualization across diverse conditions.

4) *Sim-to-real Gap Quantification*: The results for sim-to-real methods are presented in Table IV. The smaller the value, the more effective the sim-to-real method. Visualization results for photorealism enhance series are shown in Fig. 4d and for CARLA2Real series are shown in Fig. 4e and Fig. 4f. The enhanced images exhibit lower SEDD₁ and SEDD₂ values, indicating that our proposed method effectively quantifies the impact of sim-to-real translation.

TABLE IV
EXPERIMENTS FOR SIM-TO-REAL METHODS

Sim-to-real Methods		SEDD ₁	SEDD ₂
Photo-realism Enhance	Colortransfer [23]	0.242	0.384
	CUT [24]	0.192	0.278
	EPE2Vistas [25], [46]	0.191	0.249
	EPE [25]	0.175	0.245
CARLA 2Real	Raw(CARLA) [47]	0.193	0.307
	CARLA2KITTI [26]	0.172	0.158
	CARLA2CITY [26]	0.135	0.170

5) *Generalization*: Experiments are conducted on real dataset nuScenes [45], synthetic dataset SHIFT [9] and sim-to-real method EPE2Vistas [25] (refers to the EPE method where the target dataset is Vistas [46]). None of these datasets appears in the training process, but their performances meet the expectations, indicating our generalization ability.

C. Ablation Study

We evaluated the effect of the loss function using the internal variance of the real dataset. As shown in Table V, the experimental results indicate that using a single loss function leads to an increase in the intra-class variance of the feature distributions, whereas the joint loss effectively constrains the compactness of intra-class samples. The ablation experiments further demonstrate that solely relying on $\mathcal{L}_{\text{NTXent}}$ may cause the framework to overlook intra-class consistency, highlighting the need for an explicit intra-class constraint. In contrast, optimizing \mathcal{L}_C in isolation tends to converge to a

TABLE V
ABLATION STUDY.

Settings	Variance
only $\mathcal{L}_{\text{NTXent}}$	0.250
only \mathcal{L}_C	0.230
$\mathcal{L}_{\text{total}}$	0.224

local optimum, while the inter-class information provided by the contrastive loss helps mitigate it.

D. Hyperparameter Experiment

Table VI presents the results of varying the temperature τ and the loss function balancing factor λ . The results are expressed as ‘real dataset variance / center distance between synthetic and real datasets’. The degree of intra-class aggregation is represented by the variance of real dataset, where a smaller value is preferable. The degree of inter-class separation is measured by the distance between the centers of the Virtual KITTI and the real dataset. The final model is a trade-off between the intra-class aggregation and inter-class separation.

TABLE VI
HYPERPARAMETER EXPERIMENT

$\tau \backslash \lambda$	0.2	0.5	1.0
0.010	0.250 / 0.363	0.245 / 0.361	0.256 / 0.391
0.015	0.228 / 0.306	0.224 / 0.304	0.228 / 0.318
0.030	0.217 / 0.263	0.214 / 0.264	0.215 / 0.271

V. CONCLUSION

In this work, we propose a novel style-based profiling framework with a metric, Style Embedding Distribution Discrepancy (SEDD). Using a ResNet-based feature extractor, our approach derives style embeddings through Gram matrices and optimizes them with metric learning, enabling similarity quantification between synthetic and real datasets. Experiments validate the effectiveness of the proposed metric. This work transforms the synthetic-to-real gap into quantifiable objective indicators, eliminating reliance on subjective experience. It provides a standardized profiling-based tool for the quality control of synthetic datasets in autonomous driving, facilitating more targeted improvements. Future work could extend this framework to generative model-based synthetic datasets, such as world model related work.

REFERENCES

- [1] H. Liu, Z. Cao, X. Yan, S. Feng, and Q. Lu, “Autonomous vehicles: A critical review (2004-2024) and a vision for the future,” *Authorea Preprints*, 2025.
- [2] H. Zhao, Y. Wang, T. Bashford-Rogers, V. Donzella, and K. Debattista, “Exploring generative ai for sim2real in driving data synthesis,” in *2024 IEEE Intelligent Vehicles Symposium (IV)*. IEEE, 2024, pp. 3071–3077.
- [3] S. S. Ulhas, S. Kannapiran, and S. Berman, “Gan-based domain adaptation for creating digital twins of small-scale driving testbeds: Opportunities and challenges,” in *2024 IEEE Intelligent Vehicles Symposium (IV)*. IEEE, 2024, pp. 137–143.
- [4] Z. Song, Z. He, X. Li, Q. Ma, R. Ming, Z. Mao, H. Pei, L. Peng, J. Hu, D. Yao *et al.*, “Synthetic datasets for autonomous driving: A survey,” *IEEE Transactions on Intelligent Vehicles*, vol. 9, no. 1, pp. 1847–1864, 2023.

[5] S. R. Richter, V. Vineet, S. Roth, and V. Koltun, "Playing for data: Ground truth from computer games," in *Computer Vision–ECCV 2016: 14th European Conference, Amsterdam, The Netherlands, October 11–14, 2016, Proceedings, Part II 14*. Springer, 2016, pp. 102–118.

[6] G. Ros, L. Sellart, J. Materzynska, D. Vazquez, and A. M. Lopez, "The synthia dataset: A large collection of synthetic images for semantic segmentation of urban scenes," in *Proceedings of the IEEE conference on computer vision and pattern recognition*, 2016, pp. 3234–3243.

[7] A. Gaidon, Q. Wang, Y. Cabon, and E. Vig, "Virtual worlds as proxy for multi-object tracking analysis," in *Proceedings of the IEEE conference on computer vision and pattern recognition*, 2016, pp. 4340–4349.

[8] Y. Cabon, N. Murray, and M. Humenberger, "Virtual kitti 2," *arXiv preprint arXiv:2001.10773*, 2020.

[9] T. Sun, M. Segu, J. Postels, Y. Wang, L. Van Gool, B. Schiele, F. Tombari, and F. Yu, "Shift: a synthetic driving dataset for continuous multi-task domain adaptation," in *Proceedings of the IEEE/CVF Conference on Computer Vision and Pattern Recognition*, 2022, pp. 21371–21382.

[10] P. Shyam, S. Mishra, K.-J. Yoon, and K.-S. Kim, "Infra sim-to-real: An efficient baseline and dataset for infrastructure based online object detection and tracking using domain adaptation," in *2022 IEEE Intelligent Vehicles Symposium (IV)*. IEEE, 2022, pp. 1393–1399.

[11] C. Hu, S. Hudson, M. Ethier, M. Al-Sharman, D. Rayside, and W. Melek, "Sim-to-real domain adaptation for lane detection and classification in autonomous driving," in *2022 IEEE Intelligent Vehicles Symposium (IV)*. IEEE, 2022, pp. 457–463.

[12] A. Hore and D. Ziou, "Image quality metrics: Psnr vs. ssim," in *2010 20th international conference on pattern recognition*. IEEE, 2010, pp. 2366–2369.

[13] Z. Wang, A. C. Bovik, H. R. Sheikh, and E. P. Simoncelli, "Image quality assessment: from error visibility to structural similarity," *IEEE transactions on image processing*, vol. 13, no. 4, pp. 600–612, 2004.

[14] R. Zhang, P. Isola, A. A. Efros, E. Shechtman, and O. Wang, "The unreasonable effectiveness of deep features as a perceptual metric," in *Proceedings of the IEEE conference on computer vision and pattern recognition*, 2018, pp. 586–595.

[15] M. Heusel, H. Ramsauer, T. Unterthiner, B. Nessler, and S. Hochreiter, "Gans trained by a two time-scale update rule converge to a local nash equilibrium," *Advances in neural information processing systems*, vol. 30, 2017.

[16] S. Gao, S. Paulissen, M. Coletti, and R. Patton, "Quantitative evaluation of autonomous driving in carla," in *2021 IEEE Intelligent Vehicles Symposium Workshops (IV Workshops)*. IEEE, 2021, pp. 257–263.

[17] C. Zhang and A. Eskandarian, "A quality index metric and method for online self-assessment of autonomous vehicles sensory perception," *IEEE Transactions on Intelligent Transportation Systems*, vol. 24, no. 12, pp. 13801–13812, 2023.

[18] Z. Song, D. Yao, R. Ming, L. Peng, D. Yao, and Y. Zhang, "Synthetic dataset evaluation based on generalized cross validation," *arXiv preprint arXiv:2509.11273*, 2025.

[19] A. Mittal, A. K. Moorthy, and A. C. Bovik, "No-reference image quality assessment in the spatial domain," *IEEE Transactions on image processing*, vol. 21, no. 12, pp. 4695–4708, 2012.

[20] H. Talebi and P. Milanfar, "Nima: Neural image assessment," *IEEE transactions on image processing*, vol. 27, no. 8, pp. 3998–4011, 2018.

[21] W. Zhang, K. Ma, G. Zhai, and X. Yang, "Uncertainty-aware blind image quality assessment in the laboratory and wild," *IEEE Transactions on Image Processing*, vol. 30, pp. 3474–3486, 2021.

[22] A. Geiger, P. Lenz, C. Stiller, and R. Urtasun, "Vision meets robotics: The kitti dataset," *The international journal of robotics research*, vol. 32, no. 11, pp. 1231–1237, 2013.

[23] E. Reinhard, M. Adikhmin, B. Gooch, and P. Shirley, "Color transfer between images," *IEEE Computer graphics and applications*, vol. 21, no. 5, pp. 34–41, 2001.

[24] T. Park, A. A. Efros, R. Zhang, and J.-Y. Zhu, "Contrastive learning for unpaired image-to-image translation," in *Computer Vision–ECCV 2020: 16th European Conference, Glasgow, UK, August 23–28, 2020, Proceedings, Part IX 16*. Springer, 2020, pp. 319–345.

[25] S. R. Richter, H. A. AlHajja, and V. Koltun, "Enhancing photorealism enhancement," *IEEE Transactions on Pattern Analysis and Machine Intelligence*, vol. 45, no. 2, pp. 1700–1715, 2022.

[26] S. Pasios and N. Nikolaidis, "Carla2real: a tool for reducing the sim2real gap in carla simulator," *arXiv preprint arXiv:2410.18238*, 2024.

[27] M. Cordts, M. Omran, S. Ramos, T. Rehfeld, M. Enzweiler, R. Benenson, U. Franke, S. Roth, and B. Schiele, "The cityscapes dataset for semantic urban scene understanding," in *Proceedings of the IEEE conference on computer vision and pattern recognition*, 2016, pp. 3213–3223.

[28] N. Gadipudi, I. Elamvazuthi, M. Sanmugam, L. I. Izhar, T. Prasetyo, R. Jegadeeshwaran, and S. S. A. Ali, "Synthetic to real gap estimation of autonomous driving datasets using feature embedding," in *2022 IEEE 5th International Symposium in Robotics and Manufacturing Automation (ROMA)*. IEEE, 2022, pp. 1–5.

[29] X. Li, Y. Zhang, Y. Shi, H. Zhu, J. Hu, and L. Peng, "Quality assessment of image dataset for autonomous driving," in *2023 IEEE International Conference on Imaging Systems and Techniques (IST)*. IEEE, 2023, pp. 1–6.

[30] A. Duminiil, S.-S. Ieng, and D. Gruyer, "A comprehensive exploration of fidelity quantification in computer-generated images," *Sensors*, vol. 24, no. 8, p. 2463, 2024.

[31] P. Mohanaiah, P. Sathyaranayana, and L. GuruKumar, "Image texture feature extraction using glcm approach," *International journal of scientific and research publications*, vol. 3, no. 5, pp. 1–5, 2013.

[32] S. Ke-Chen, Y. Yun-Hui, C. Wen-Hui, and X. Zhang, "Research and perspective on local binary pattern," *Acta Automatica Sinica*, vol. 39, no. 6, pp. 730–744, 2013.

[33] D. Zhang, "Wavelet transform," in *Fundamentals of image data mining: Analysis, Features, Classification and Retrieval*. Springer, 2019, pp. 35–44.

[34] A. Duminiil, S.-S. Ieng, and D. Gruyer, "Assessing fidelity in synthetic datasets: A multi-criteria combination methodology," in *2024 27th International Conference on Information Fusion (FUSION)*. IEEE, 2024, pp. 1–8.

[35] K. He, X. Zhang, S. Ren, and J. Sun, "Deep residual learning for image recognition," in *Proceedings of the IEEE conference on computer vision and pattern recognition*, 2016, pp. 770–778.

[36] J. Deng, W. Dong, R. Socher, L.-J. Li, K. Li, and L. Fei-Fei, "Imagenet: A large-scale hierarchical image database," in *2009 IEEE conference on computer vision and pattern recognition*. Ieee, 2009, pp. 248–255.

[37] L. Van der Maaten and G. Hinton, "Visualizing data using t-sne," *Journal of machine learning research*, vol. 9, no. 11, 2008.

[38] S. Lee, T. Son, and S. Kwak, "Fifo: Learning fog-invariant features for foggy scene segmentation," in *Proceedings of the IEEE/CVF Conference on Computer Vision and Pattern Recognition*, 2022, pp. 18911–18921.

[39] D. Shim and H. J. Kim, "Divide: Learning a domain-invariant geometric space for depth estimation," *IEEE Robotics and Automation Letters*, 2024.

[40] L. A. Gatys, A. S. Ecker, and M. Bethge, "Image style transfer using convolutional neural networks," in *Proceedings of the IEEE conference on computer vision and pattern recognition*, 2016, pp. 2414–2423.

[41] Y. Wen, K. Zhang, Z. Li, and Y. Qiao, "A discriminative feature learning approach for deep face recognition," in *European conference on computer vision*. Springer, 2016, pp. 499–515.

[42] H. Xuan, A. Stylianou, and R. Pless, "Improved embeddings with easy positive triplet mining," in *Proceedings of the IEEE/CVF Winter Conference on Applications of Computer Vision*, 2020, pp. 2474–2482.

[43] T. Chen, S. Kornblith, M. Norouzi, and G. Hinton, "A simple framework for contrastive learning of visual representations," in *International conference on machine learning*. PmlR, 2020, pp. 1597–1607.

[44] A. Gretton, K. M. Borgwardt, M. J. Rasch, B. Schölkopf, and A. Smola, "A kernel two-sample test," *The Journal of Machine Learning Research*, vol. 13, no. 1, pp. 723–773, 2012.

[45] H. Caesar, V. Bankiti, A. H. Lang, S. Vora, V. E. Lio, Q. Xu, A. Krishnan, Y. Pan, G. Baldan, and O. Beijbom, "nuscenes: A multimodal dataset for autonomous driving," in *Proceedings of the IEEE/CVF conference on computer vision and pattern recognition*, 2020, pp. 11621–11631.

[46] G. Neuhold, T. Ollmann, S. Rota Bulo, and P. Kortschieder, "The mapillary vistas dataset for semantic understanding of street scenes," in *Proceedings of the IEEE international conference on computer vision*, 2017, pp. 4990–4999.

[47] A. Dosovitskiy, G. Ros, F. Codevilla, A. Lopez, and V. Koltun, "Carla: An open urban driving simulator," in *Conference on robot learning*. PMLR, 2017, pp. 1–16.